Manuscript title: A Sentinel-2 based multi-temporal monitoring framework for wind and bark beetle detection and damage mapping

Manuscript type: Article

Authors: Anna Candotti[1,2,*], Michaela De Giglio[1], Marco Dubbini[1] and Enrico Tomelleri[2]

[1] Department of History and Cultures (DiSCi)-Geography Section, University of Bologna, Via Guerrazzi 20, 40125 Bologna, Italy; anna.candotti@natec.unibz.it; michaela.degiglio@unibo.it; marco.dubbini@unibo.it
[2] Faculty of Science and Technology, Free University of Bolzano, Piazza Università 5, 39100 Bolzano, Italy; anna.candotti@natec.unibz.it; enrico.tomelleri@unibz.it
* Correspondence

A Sentinel-2 based multi-temporal monitoring framework for wind and bark beetle detection and damage mapping

Anna Candotti[1,2,*], Michaela De Giglio[1], Marco Dubbini[1] and Enrico Tomelleri[2]

[1] Department of History and Cultures (DiSCi)-Geography Section, University of Bologna, Via Guerrazzi 20, 40125 Bologna, Italy; anna.candotti@natec.unibz.it; michaela.degiglio@unibo.it; marco.dubbini@unibo.it
[2] Faculty of Science and Technology, Free University of Bolzano, Piazza Università 5, 39100 Bolzano, Italy; anna.candotti@natec.unibz.it; enrico.tomelleri@unibz.it
* Correspondence

Abstract: The occurrence of extreme windstorms and increasing heat and drought events induced by climate change leads to coniferous forests showing severe damage and stress and making trees more vulnerable to spruce bark beetle infestations. The combination of abiotic and biotic disturbances in forests can cause drastic environmental and economic losses. The first step for containing such damage is the establishment of a monitoring framework for early detection of vulnerable plots and distinguishing the cause of forest damage at the scale from management unit to region. For developing and evaluating the functionality of such a monitoring framework, we first selected an area of interest affected by wind throw damages and bark beetles at the border between Italy and Austria in the Friulian Dolomites, Carnic and Julian Alps and the Carinthian Gailtal. Secondly, we implemented a framework for time-series analysis with open access Sentinel-2 data over four years (2017-2020) by quantifying single band sensitivity to disturbances. Additionally, we enhanced the framework by deploying vegetation indices, for monitoring spectral changes and performing supervised image classifications for change detection. A mean overall accuracy of 89% was achieved, thus Sentinel-2 imagery proved to be suitable for distinguishing stressed stands, bark beetle attacked canopies and wind fell patches. The advantages of our methodology are its global, large-scale and "FAIR" principles compliant applicability to monitor forest health, forest cover change and its usability to support the development of forest management strategies for dealing with massive bark beetle outbreaks.

Keywords: forests; spruce bark beetle; windstorms; drought; remote sensing; Sentinel-2; spectral signatures; vegetation indices; supervised image classification; forest cover change detection

1. Introduction

Due to ongoing global climate change, forest ecosystems are increasingly exposed to unfavourable environmental conditions such as droughts and cold spells. Such changes are linked to contemporaneously rising temperatures and changing precipitation patterns [1]. At the same time, the frequency of disturbances such as major wind throws, and snow damages expose forest ecosystems to an increase in the frequency and severity of biotic damages [1]. Thus, native, and alien insects, fungi and nematodes infestations are expected to be a major threat for European forests in the next future [1]. In this context, the homogeneity of even-aged monoculture stands of Norway spruce (*Picea abies*) is a favourable condition for the diffusion of the European spruce bark beetle (*Ips typographus*) [2]. Increasing stress conditions of such forest stands supported the uncontrolled growth of the bark beetle population to epidemic proportions to the point that the insect has already destroyed more forested

areas than any other natural disturbance [2, 3]. Spruce bark beetle infestations are affected by rising temperatures due to the exothermic physiology of the insects and the drought sensitivity of the defence system of trees [4].

Female beetles drill egg galleries under the bark. Later, larvae emerge and feed in phloem before changing into pupae. The adults may move on to another host two to five weeks after the attack. The larvae feed in the phloem after hatching and pupate beneath the bark [1]. Each year, up to three generations are possible [1]. Successful beetle colonization of a healthy tree is typically fatal, because hundreds of beetle attacks destroy the inner bark and disrupt nutrient transport to the roots. [1]. If this increase in mortality persists for a more extended period, large patches of forest could be affected with a consequently altered forest structure and composition and losses of biodiversity and ecosystem services provision (e.g., hydrological regulation and carbon storage capacity) [5]. To prevent massive outbreaks and to minimise economic losses induced by a range of cascading impacts on markets, like oversupply and decreasing timber prices, early detection of infestations is crucial, that is, before the infestation is visible on the ground [6]. Management measures successfully applied in the past are becoming inefficient under a warmer climate, particularly in forests dominated by Norway spruce, because of their lower resistance to drought stress. On the other hand, forests managed for diversity showed lower disturbance rates [7].

A prerequisite for effective management is understanding forest damage's spatial distribution and severity. From a forestry perspective, detecting outbreaks at the initial stage is the most important, as the management aims to preclude a mass outbreak by sanitation harvesting [8]. The phenology of bark beetle attacks can be divided into three stages: green, red and grey-attack with varying degrees of visibility [9,10]. These stages were named after the characterising the foliage colour, which is related to the time from the phloem damage [9, 10].

The infested trees in a managed forest are traditionally located during field surveys, but the method is laborious and hardly applicable to large or inaccessible areas [11]. An important new management strategy might be to reduce risks by looking at the whole landscape configuration rather than at single stands in order to account for measures that also foster forest resilience at ecosystem level [12]. Remote sensing data are useful for detecting and monitoring areas infested by spruce bark beetles as they provide global, spatially continuous, and periodic data on vegetation conditions [13]. Remote sensing data can also reduce costs associated with field observations, as there are many freely available data sources with global coverage and regular revisit times like Sentinel-2 [14]. The availability of high-quality (i.e., cloud-free) Sentinel-2 images is an important prerequisite for the successful monitoring of bark beetle damage dynamics, as these show high variability in space and time [15]. Accurate estimates of leaf pigments, nitrogen, dry matter, and water content from remote sensing can assist in determining vegetation physiological status and serve as bio-indicators of vegetation stress [17, 18]. Einzmann et al. [19] found that in an artificially induced stress experiment on Norway spruce, the spectra of stressed trees differed significantly from the mean of the control trees. In contrast, the control tree spectral signature did not change over time. Compared to the mean of the control trees, both the needle and the canopy reflectance of artificially stressed trees increased in the visible (mainly red) and SWIR range, while a decrease was observed in the Near Infrared (NIR) range. Furthermore, a slight decrease in the Red-Edge Inflection Point (REIP) was observed. The primary and secondary effects of water content on leaf reflectance showed that the sensitivity of leaf reflectance to water content is greatest in spectral bands in the SWIR region [18]. These changes are caused by a typical reaction to vitality losses and cell structure alteration when chlorophyll and leaf water are reduced. In addition to altered leaf optical properties, needle loss affects canopy scale spectral signatures [19]. Both the changes in photosynthetic activity of green leaves, and water content changes triggered by bark beetle can be detected from early infestation stages using imaging spectroscopy. The resolution of Sentinel-2 imagery was demonstrated to advantageous for such purposes [20]. An overall accuracy of 67% in detecting the bark beetle green attack stage with Sentinel-2 data was obtained for 2016 in the Bavarian Forest National Park without relying on field data but only on visual image interpretation of aerial photographs taken in the year following the attack [20]. Reflectance changes of infested Norway spruce trees were observable especially in the Red-Edge and SWIR regions as well as in vegetation indices calculated from those bands such as such as the Normalised Difference Red Edge Index

(NDREI) and the Normalised Difference Water Index (NDWI), both for leaf and canopy levels [20, 21]. A research from 2020 showed that Sentinel-2 data were able to accurately distinguish the areas under bark beetle disturbances and to detect the individual phases of the recovery mode of the forest vegetation using the Normalised Difference Vegetation Index (NDVI), the Normalize Difference Moisture Index (NDMI) and Tasseled Cap Wetness (TCW) during the period of 2017 to 2019 in the Low Tatras National Park (Slovakia) and the Sumava National Park (Czech Republic) [22]. The reflectance of the healthy forest vegetation was higher in the NIR band than in the SWIR; however, the SWIR reflectivity was higher in the case of bark beetle disturbances. This aspect played an important role as the SWIR bands responded sensitively in the case of the degradation of the forest [22]. Spectral changes of healthy and attacked spruce monoculture stands within a single vegetation season were monitored in the Bohemian–Moravian Highlands (Czech Republic) using dense time series of Sentinel-2 satellite observations to identify the most sensitive spectral bands and vegetation indices for early detection of bark beetle infestation [15]. The highest potentials for separation between the healthy and infestation classes were observed for the Red, Red-Edge and SWIR regions of the spectrum with an overall accuracy of 78%. In this study [15], NIR bands seemed less appropriate for early bark beetle detection, despite the recent evidence from Abdullah et al. [20] pointing to significant differences in NIR leaf-level spectra between healthy and infested trees. Spectral indices using Red-Edge and Short-Wave Infrared might be potentially useful to detect infestation even earlier than indices based solely on VIS/NIR region [15, 23]. Approaches based on multi-temporal spectral analysis have proven to be the most effective to detect bark beetle infestations at an early stage with Sentinel-2 data [14-16, 22-24].

Hereby, we propose a new multi-temporal framework for regional scale wind and bark beetle damage mapping from Sentinel-2 imagery and field surveys. In doing this, we first evaluate the detection of early stages of bark beetle attacks on Norway spruce stands over four years (2017-2020) by tracking theirs within-season changes of canopy reflectance. Individual spectral bands and vegetation indices were used to develop a supervised image classification model in order to separate between classes of healthy, stressed, "red_attack" stage or windstorm-damaged stands over an area of 1 000 000 ha of which 120 000 ha are covered by Norway spruce. Lastly, the results were validated with field reference data and implemented for the analysis of forest cover change by post-classification change detection over the time-series, in relation to both spruce bark beetles' infestations and windstorm damages.

2. Materials and Methods

2.1. Study Area

The chosen study site for bark beetle detection and analysis of forest cover change (2017-2020) is located at the border between Italy, Austria, and Slovenia in the Friulian Dolomites, Carnic and Julian Alps and the Carinthian Gailtal (Fig. 1). In Friuli Venezia Giulia, Norway spruce is the main forest species, covering about 66,100 ha scattered in seven main types of mixed and pure forests. The other common diffused tree species are: European beech, Silver fir as well as Black and Scots pine [25]. Typical pure and even aged spruce forest grow on fertile soils from 1000 to 1500 m a.s.l. and non-native even aged spruce forests, sometimes mixed with natural spruce reforestation (secondary stands), grow from 800 to 1600 m a.s.l., in abandoned pastures. Several areas got replanted with Norway spruce deriving from market-oriented reforestation management of the XX century. There has been a recent low altitude spruce reforestation with pure and even-aged spruce plantations normally growing in small stands from 200 to 800 m a.s.l in areas that are dominated by broadleaved species [26]. Also, for the Carinthian side of the study area, Norway spruce, followed by Silver fir, Black and Scots pine, European beech and Larch are the main tree species [27]. For the purpose of this study, only sites of the study area with Norway spruce stands (pure or mixed), were considered (Fig. 1).

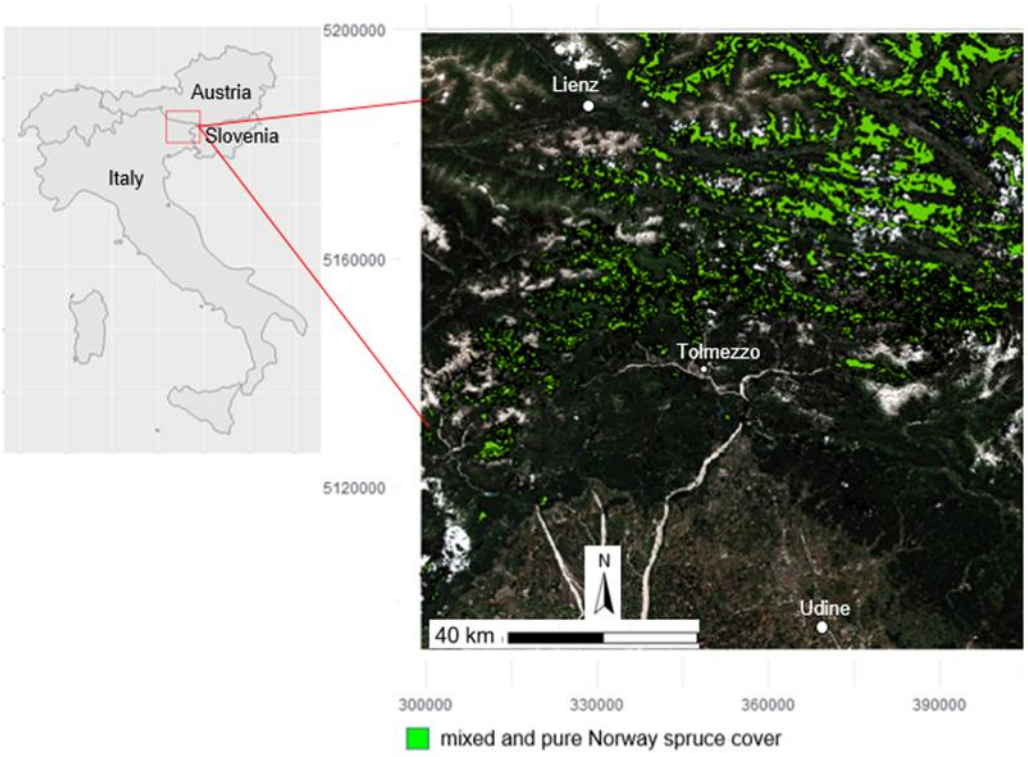

Figure 1. Location of study area and RGB from Sentinel-2 of July 2020 with polygons in green representing mixed and pure Norway spruce stands. Reference system: WGS84-UTM33N.

Mountain areas of the study area are characterized, at lower latitudes, by high medium annual precipitation rates (2700-3200mm), while in the internal alpine area they only amount to ca. 1500mm. Average annual air temperature ranges between 6 and 10 °C [28,29]. Regarding average annual climate conditions of the study region, 2018 was very hot and dry having a mean temperature of 13 °C in mountain areas, while 2019 and 2020 had a mean temperature of 10°C [30, 31, 32]. Nevertheless, both years 2019 and 2020 were characterized by an annual temperature anomaly of 1°C for 2019 and of 2.4 °C for 2020 compared to the last two decades [31,32]. Spring average precipitation have the strongest impact on bark beetle population development [33]. While the spring months of 2018 showed a mean increase in precipitation of 20-40% compared to the average values of 1961- 2010 [30,34], spring (including June) of 2019 was 20-50% drier than usual [31]. March and April 2020 were even 60-80% drier than the reference period [32].

2.1.1. The Vaia storm

The Vaia storm hit the North-Eastern part of Italy and Southern Austria on between the 28 and 29 October 2018 with winds exceeding 200 km/h and strong rainfall [35]. It caused extensive forest damage in 494 Italian municipalities, destroying or severely damaging forests of about 42 500 ha, with an estimated damage of 9.6 million of cubic meters across an area of 42500 ha [35]. For the Friuli Venezia Giulia region, estimates of the forest damage were provided by the local forest service using aerial photographs and ground surveys which estimated that a surface extending 3700 ha was damaged and the volume affected by the storm being of 780 000 cubic meters [35]. In Carinthia Vaia caused 1.5 million cubic meters of damaged wood [30]. Vaia mostly affected pure and mixed Norway spruce stands, as their roots are relatively superficial and prone to uprooting [36]. In forest stands where trees were more diversified in age and species, devastating effects of the wind were more restricted, with a better resistance due to different morphology of the root system [36].

2.2. Data

We made use of satellite imagery to detect forest stress due to bark beetle attacks and to monitor forest change over the study period. For this purpose, we made use of Sentinel-2A and Sentinel-2B images in the form of Level-2A products (atmospherically corrected to bottom-of-atmosphere reflectance) [37]. We collected Sentinel-2 tiles with the R package "getSpatialData" (version 0.1.0) selecting images with cloud cover inferior to 10%. Images were cropped to the area of interest and bands with original resolution of 20 m x 20 m (B05, B06, B07, B11, B12) were resampled to 10m x 10m pixels. We didn't make use of the bands with a 60 m spatial resolution (B01 and B09) because they are mainly relevant for atmospheric corrections [38]. The dataset was collected with a monthly time step for the period from July to September from the years from 2017 to 2020. We included May based ond data availability due to higher cloud cover in spring (Tab. 1). The timeframe was chosen according to the bark beetle life cycle phenology study area, which begins in May by overwintered beetles, and expands in July for the second generation, and ends in September. The attacked trees are initially stressed ("green_attack") and later encounter a browning process which timing is diverse depending on the time of the year in which the trees got initially attacked. The culmination of such browning process is commonly called "red_attack". Stands attacked in May, usually start to show visible symptoms like needle loss and initial discoloration in July, while those infested in summer show "red_attack" symptoms in the following spring [39]. Forest cover masks were obtained from the Copernicus Land Monitoring Service [40], which provides tree cover density (TCD) and dominant leaf type (DLT) indicating broadleaf or needle-leaf majority. These datasets are available with 20m resolution starting from the year 2018. Secondly, we merged such datasets with the forest cover polygons – which includes the dominant tree species - from the Autonomous Region Friuli Venezia Giulia and Land Kärnten to increase the accuracy and to include the specific forest cover type.

We gathered information about the bark beetle population counts from pheromone traps in Friuli Venezia Giulia for the years from 2017 to 2020 (Fig. 2). This dataset provided by the Regional Agency for Rural Development (ERSA FVG) contains the location and altitude of the trap, its installation date, captures per week and total captures. Bark beetle captures by pheromone traps in the northern part of the Region showed an increase in population und diffusion in 2019, especially related to areas covered by windfelled trees [41]. For the Austrian side of the study area, we used the the PHENIPS model and trap captures from the Austrian Federal Forest Office (BFW) [42]. Additionally, we included polygons of sites damaged by bark beetle infestations with information about stand species and age and volume of damaged trees and polygons representing windfelled sites from the Vaia storm of 2018, located during field surveys and provided by the Regional Forestry Service - Friuli Venezia Giulia and the Carinthian Institute for Geographic Information Systems (KAGIS) (Fig. 2). Orthofotos from 2017-2020 provided by the Regional Infrastructure of Environmental and Terriorial Data (Irdat FVG) [43], were used for photointerpretation of wind felled areas and sites affected by bark beetle damage. We extracted the topographic parameters from a digital elevation model (Global Digital Elevation Model from the NASA Earth Data Portal) [44] for the areas affected by bark beetle attack and wind damage. Additionally, we exploited the Soil Water Index (SWI) from the Copernicus Global Land Service [40] to quantify the moisture condition. Moreover, we gathered Land Surface Temperature (LST) data from the Sentinel-3 mission from the Copernicus Open Access Hub [45]. We carried out the analysis for this study with the R programming language (version 4.1.2).

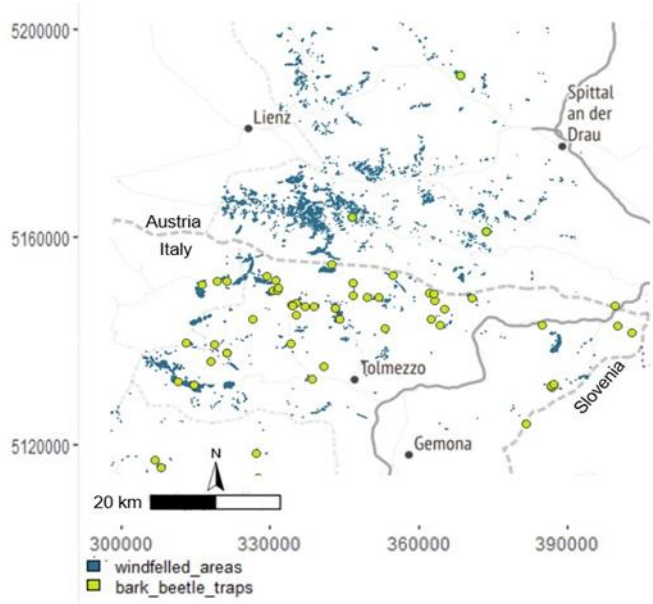

Figure 2. Reference data distribution over the study area showing the location of bark beetle pheromone traps and wind fell patches. Reference system: WGS84- UTM33N.

Table 1. Sentinel-2 data**.**

Number	Date	Data
1	20/06/2017	Sentinel-2 L2A
2	02/08/2017	Sentinel-2 L2A
3	29/08/2017	Sentinel-2 L2A
4	06/05/2018	Sentinel-2 L2A
5	30/07/2018	Sentinel-2 L2A
6	17/08/2018	Sentinel-2 L2A
7	28/09/2018	Sentinel-2 L2A
8	24/05/2019	Sentinel-2 L2A
9	30/06/2019	Sentinel-2 L2A
10	27/08/2019	Sentinel-2 L2A
11	21/09/2019	Sentinel-2 L2A
13	07/07/2020	Sentinel-2 L2A
14	29/07/2020	Sentinel-2 L2A
15	15/09/2020	Sentinel-2 L2A

2.3. Methods

Cloud masks were applied for every scene according to the native cloud cover information of Sentinel-2 Level 2-A products [37] (Fig. 3). Such a mask doesn't account for shadowed areas, which can be easily distinguished by unusual high reflectance in the blue part of the spectrum. Consequently, such areas were treated as a separate class during the classification process which will be described further on.

2.3.1. Single bands and vegetation indices

Single band pixel values from Sentinel-2 images were analysed for each available acquisition date (Fig. 3) considering ground truth reference data and by photointerpretation from RGB and false colour products. Especially the reflectance trends of the NIR (B08) and SWIR (B12) bands were taken in account because those are the most sensitive ones to chlorophyll decrease (B08 band) and water stress/lower absorption rates (B12 band) [21, 15]. Training data, i.e. training polygons drawn for the

classes of healthy, stressed and "red attack" stage canopies from 2020 was used to extract spectral profiles for both bands (B08 and B12) and in order to quantify the variables´ separability and seasonal changes in time.
From the Sentinel-2 imagery, we extracted time series of vegetation indices (Fig. 3) for the growing seasons 2019 and 2020 with the objective of detecting foresting health changes using training polygons from 2020. The indices were chosen based on the bands sensitivity to stress-induced variations in chlorophyll content (VIS), biomass (NIR), and water content (SWIR). For the green-attack stage detection, especially water-content based indices are suitable like the Normalized Difference Water Index (NDWI, Eq. 1), which is dimensionless and ranges between ±1, where high values stand for high leaf water content and high vegetation cover. This index is particularly useful in early stress detection and allows to map temporal changes more accurately as it exhibits faster feedback than the Normalised Difference Vegetation Index (NDVI, Eq. 2) for decreasing leaf water content [46,47]. Additionally, NDWI is more robust to atmospheric influences as atmospheric aerosol scattering effects are stronger in the VIS spectral wavelengths [46, 47]:

$$NDWI = \frac{(NIR-SWIR2)}{(NIR+SWIR2)} \quad (1)$$

$$NDVI = \frac{(NIR-Red)}{(NIR+Red)} \quad (2)$$

Disease Water Stress Index (DWSI, Eq. 3) was calculated as it proved to be able to detect changeable climatic conditions, especially the impact of drought on forest ecosystems in case of which DWSI decreases. DWSI values range between 0 and 2.5 for forests according to a previous study and in case of pure conifers, there is a distinct difference in DWSI index for dry sites, especially for the first part of the vegetation period from April to July [48]:

$$DWSI = \frac{(NIR-Green)}{(SWIR1+Red)} \quad (3)$$

The Normalized Multi-band Drought Index (NMDI, Eq. 4) was adopted, for detecting vegetation water by using three channels centered near 860 nm, 1640 nm and 2130 nm. By combining information from multiple NIR and SWIR channels, NMDI has enhanced the sensitivity to drought severity, and is well suited to estimate water content for both soil and vegetation [47]. NMDI values are within the range of 0.7 to 1 when soil moisture is less than 0.1, which means dry soil conditions. NMDI values are around 0.6 when soil moisture is at intermediate moisture conditions. When NMDI is less than 0.6, the soil is under wet conditions. Lower NMDI values indicate increasing severity of vegetation drought [47].

$$NMDI = \frac{(NIR-(SWIR1-SWIR2))}{(NIR+(SWIR1+SWIR2))} \quad (4)$$

The Normalized Distance Red and SWIR (NDRS, Eq. 5) vegetation index, which was recently implemented to early detect forest stress from spruce bark beetle attacks was also used in this research [24]:

$$NDRS = \frac{(DRS - DRS'\min)}{(DRS'max - DRS'\min)} \quad (5)$$

where

$$DRS = \sqrt{(Red)^2 + (SWIR1)^2} \quad (6)$$

DRS'max and DRS'min are the ranges of the DRS values for all spruce pixels in the image and a threshold of 0.5 is applied to classify pixels as stressed or healthy if lower [24].

Red-Edge based vegetation indices were calculated for bark beetle detection too. Among them, the REIP (Eq. 7), as with increasing stress the abrupt transition that is normally seen between the visible and the NIR in the Red Edge range in green vegetation begins to shift towards shorter wavelengths [49]. The Normalised Difference Red Edge Index (NDREI, Eq. 8) can be applied to estimate chlorophyll concentrations minimizing the effects of background soil reflectance with values below 0.5 indicating a condition of stress [23]:

$$REIP = \frac{0.705 + 0.35\left(\frac{Red + RedEdge3}{2} - RedEdge1\right)}{RedEdge2 - RedEdge1} \quad (7)$$

$$NDREI1 = \frac{(RedEdge2 - RedEdge1)}{(RedEdge2 + RedEdge1)} \quad (8)$$

$$NDREI2 = \frac{(RedEdge3 - RedEdge1)}{(RedEdge3 + RedEdge1)} \quad (9)$$

The Red Edge Normalized Difference Vegetation Index (RENDVI, Eq. 10), also called Red Edge NDVI or NDVI 705, used to assess post fire regeneration and based on Red and Red-Edge bands in another study [50], was compared with other indexes in this study. Both the bands B04 and B05 and the bands B04 and B06 were used. In the following formula R represents the Bottom of Atmosphere (BOA) reflectance observed by the satellite sensor:

$$RENDVI = \frac{(R750nm - R705nm)}{(R750nm + R705nm)} \quad (10)$$

This index proved to be useful as it considers a narrower waveband at the edge of the chlorophyll absorption feature (e.g. 705 nm). NDVI 705 is more affected by chlorophyll content when compared to the NDVI and common applications include precision agriculture, forest monitoring, forest fires and vegetation stress detection [51].
Additionally, Tasseled Cap Wetness (TCW, Eq. 11) was calculated to further distinguish disturbed and undisturbed forest areas. To create this index, the following equation for the Sentinel-2 data, with the exact parameters from the Index Database from the University of Bonn for the Sentinel-2 data was used [52]:

$$TCW = 0.1509 * B02 + 0.1973 * B03 + 0.3279 * B04 + 0.3406 * B08 - 0.7112 * B11 - 0.4572 * B12 \quad (11)$$

TCW has previously proven to be useful for the detection of forest stands attacked by bark beetles showing negative values for infested forest sites [22].

2.3.2. Supervised classification of multi-temporal imagery

We firstly performed a supervised image classification (Fig. 3) to assign each pixel to a particular forest class of interest ("healthy", "stressed", "red_attack" or "vaia"), based on statistical characteristics of reflectance values of the training samples. Four non-parametric machine learning methods were used: Random Forest (RF), Support Vector Machine (SVM), Artificial Neural Networks (ANN) and k-Nearest Neighbors (KNN). Training polygons were manually selected based on RGB and false colour composites, as well as single band reflectance values and reference data (trap captures, areas damaged by bark beetles, wind felled areas and orthophotos) for each dataset. The training polygons were based only on reference data (Fig. 3) available at the time of the respective image acquisition and by avoiding a retrospective approach through ground truth information gathered afterwards, as it would have compromised the green-attack stage detection. At least ten polygons per class, of 30m x 30m each (3x3 pixels), were drawn. We chose the size of the training dataset based on a rule of thumb according to which a subset size of at least ten times the number of bands used during the classification (in this case 9) has to be considered for each training class [53].

The training polygons were sampled for each Sentinel-2 dataset and then split into a training (70%) and a test (30%) dataset. Spectral signatures were extracted for each date to detect a reflectance trend for each class. The classification algorithms were trained using both single bands and vegetation indices as explanatory variables, like in a recent study [15]. Variable importance was calculated in order to evaluate which explanatory variables were the most significant during the classification process in distinguishing between classes based on their reflectance values. The final accuracy of the classifications was assessed with confusion matrixes, overall accuracy and kappa coefficient (Fig. 3).

2.3.3. Post-Classification forest cover change detection

We carried out post-classification change detection (PCC) by Intensity Analysis (IA) to analyse quantitatively the Land Use Capability (LUC) maps at several time steps, using cross-tabulation matrices, where each matrix summarises the LUC change at each time interval (Fig. 3). IA evaluates in three levels the deviation between observed change intensity and hypothesised uniform change intensity. Hereby, each level details information given by the previous analysis level. First, the **interval level** indicates how size and rate of change varies across time intervals. Second, the **category level** examines for each time interval how the size and intensity of gross losses and gross gains in each category vary across categories for each time interval. Third, the **transition level** determines for each category how the size and intensity of a category's transitions vary across the other categories that are available for that transition. At each level, the method tests for stationarity of patterns across time intervals [54]. The discrete variables obtained by the results of the supervised classifications were used for this purpose. The R-package "OpenLand" (version 1.0.2) was used to calculate the number of times a pixel had changed during the analysed period. A raster with the number of changes as pixel value and a table containing the areal percentage of every pixel value (number of changes) were obtained. Further, calculation of differences in frequencies of pixels assigned per class for each dataset was performed and changes in land cover area per class plotted to visualise changes in forest cover before and after the Vaia storm occurred and how it affected bark beetle infestations. Finally, we used classification maps from 2017 until 2020 for evaluating two focus areas, showing relevant changes in forest cover and health.

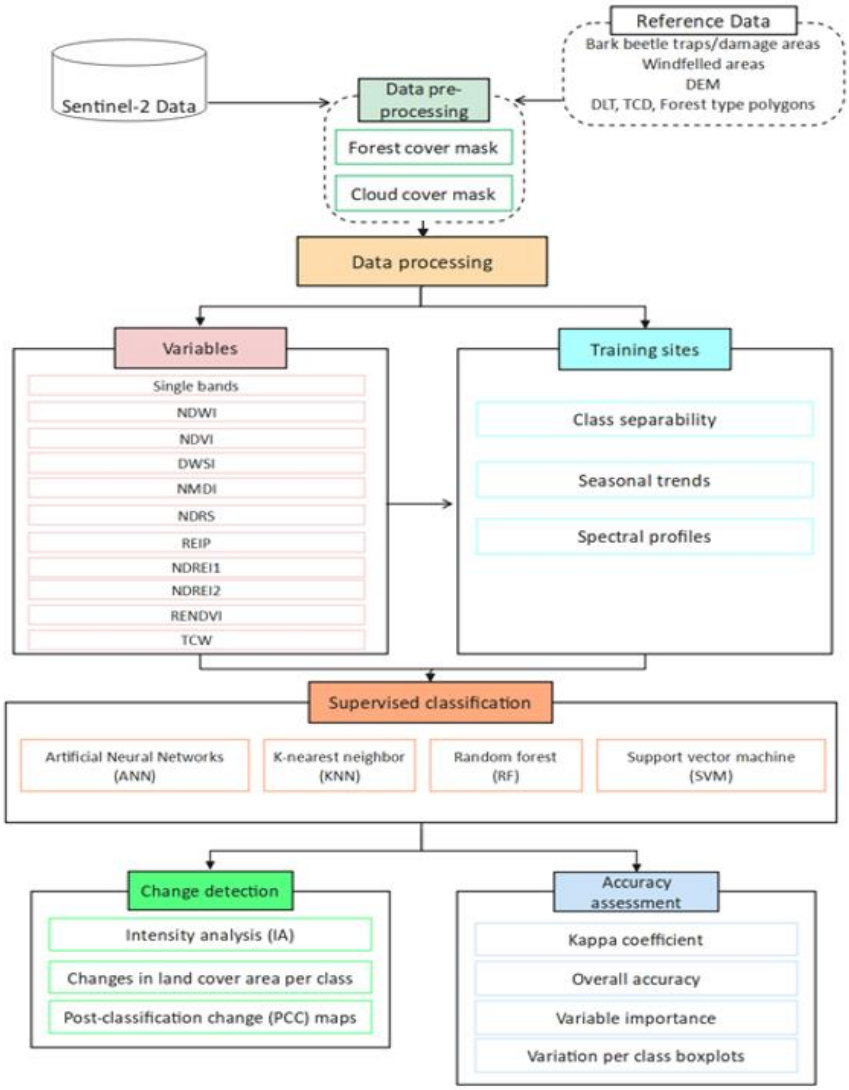

Figure 3. Workflow diagram**.**

3. Results

3.1. Single band and vegetation indices reflectance values

The results obtained from single band change detection over time using training data from 2020, showed that in the NIR band (B08), (Fig. 4, A) and in the SWIR band (B12), (Fig. 4, B) there is a significant variation in reflectance within areas damaged by bark beetles compared to reflectance values of healthy forest stands. The differences between healthy and stressed stands on the other hand are more significant in the B08 band, with values of the stressed sites being more similar to the spectral profile of stands under bark beetle "red_attack" stage than to the healthy ones (Fig. 4, A). Also healthy stands displayed a seasonal variation in reflectance with increasing values until July (2019) or August (2020) and decreasing values from summer to early autumn (September 2019 and 2020). Considering the seasonal reflectance of the summer months in the B08 band, while healthy stands witnessed a significant increase in NIR reflectance, the stands of stressed and "red_attack" sites only showed a slight increase in reflectance (Fig. 4, A). In the B12 band, forest stands under bark beetle "red_attack" stage can clearly be distinguished showing higher reflectance values, while healthy and stressed stands had very similar spectral responses for both seasons. Nevertheless, a slight increase in reflectance was observed in stressed stands beginning from August 2020 compared to the values of healthy stands (Fig.

4, B). Stands identified as under bark beetle-red attack stage in 2020 already showed significantly deviating values in 2019 compared to the healthy canopies for both bands (Fig. 4, A and B). Forest areas selected as stressed according to training data from 2020, exhibited similar spectral responses for both 2019 and 2020, however with overall lower values in 2020 in the B08 band (Fig. 4, A) and higher reflectance in August and September 2020 in the B12 band (Fig. 4, B).

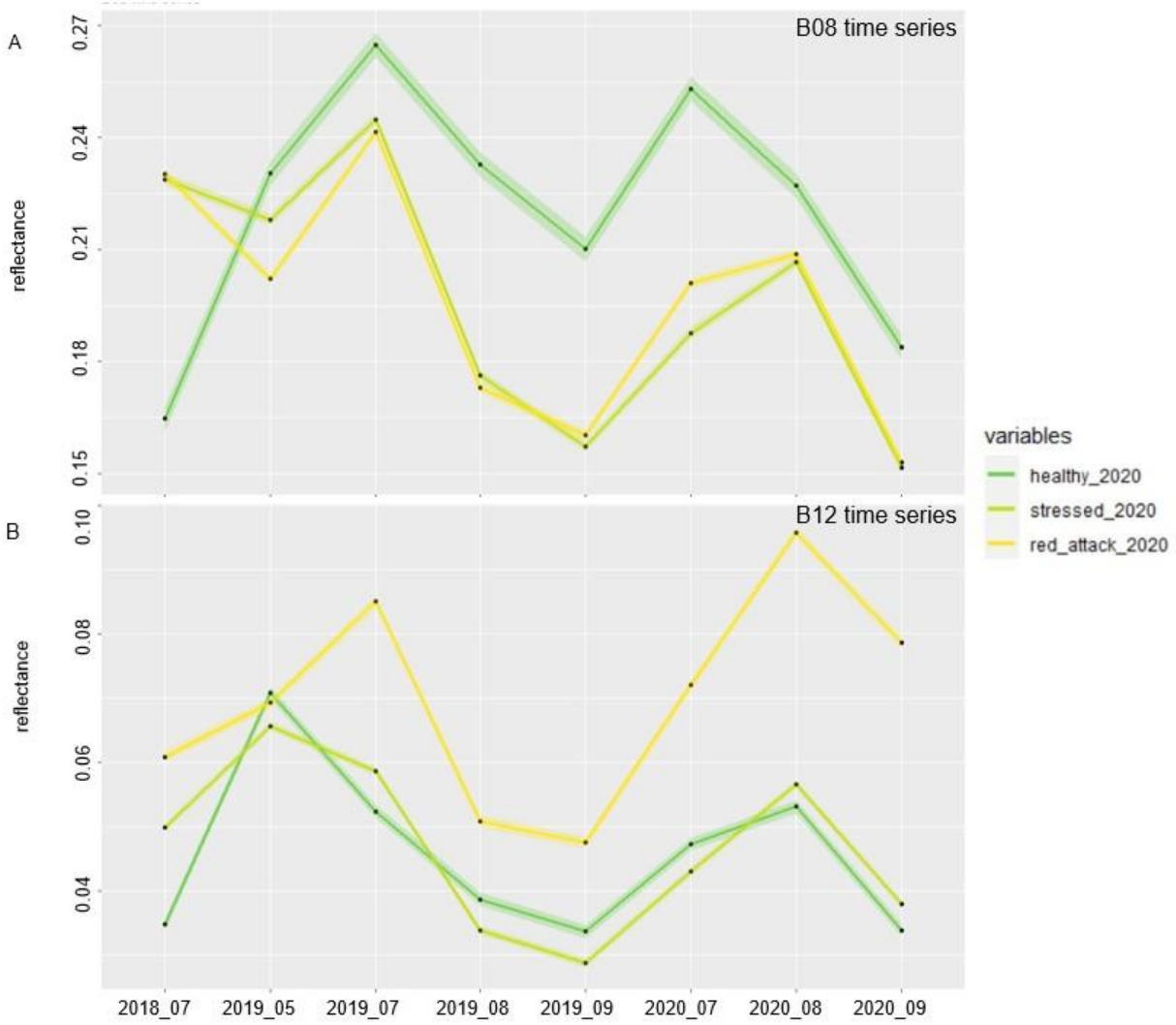

Figure 4. Mean seasonal B08 (A) and B12 (B) band reflectance (line) and standard error (confidence band) in a time series from 2018 to 2020 for healthy, stressed and red—attack stage canopies using training data from 2020.

The vegetation indices NDWI, DWSI, NMDI, NDRS, NDREI2 and TCW, among the ten that were later considered for the classifications, were found to be suitable to successfully distinguish healthy and stressed or damaged forest stands. The most frequently used band for those indices is the B12 band. The reported indices further rely on the B08 band, the B05, B06, B07 (Red Edge bands), the B03 (Green band) and/or the B04 (Red band). For all vegetation indices and for both considered seasons, the values of healthy and stressed stands are more similar to each other compared to forests under "red_attack" bark beetle infestation, which showed very significant differences (Fig. 5). For normalised indices (NDWI, NDMI and NDREI2), in all cases, the healthy stands displayed the highest values followed by the samples from stressed stands and with the lowest values for the stands

under bark beetle "red-attack" stage (Fig. 5, A, B and E). NDRS was found to have very similar values for healthy and stressed stands, while forest stands under "red_attack" stage resulted in significantly higher values (Fig. 5, D). TCW exibited positive values for healthy stands, values between 0 and -250 for stressed stands and an even lower range (between -125 and -625) for "red_attack" stage canopies (Fig. 5, F). NDWI, NMDI, DWSI and TCW showed the largest difference between healthy and stressed pixels (Fig. 5, A, B, C and F). While healthy and stressed stands showed very similar seasonal trends for both seasons, stands already in the "red-attack" stage in 2020 showed the most significant decreases beginning in July 2020 for NDWI, NMDI, DWSI and NDREI2, compared to the values of 2019 (Fig. 5, A, B, C and E). However, both stressed and "red_attack" stage canopies from 2020, already showed deviating values in 2019 compared to the reflectance of healthy crowns (Fig. 5). The seasonal trajectories showed reflectance changes in absolute values from one year to another independently from bark beetle infestations (also healthy forest stands were affected), which indicates that an absolute threshold of discrimination between classes cannot be applied, and that the specific seasonal reflectance of healthy forests stands should rather be used as a reference baseline to differentiate between the variables (Fig. 5).

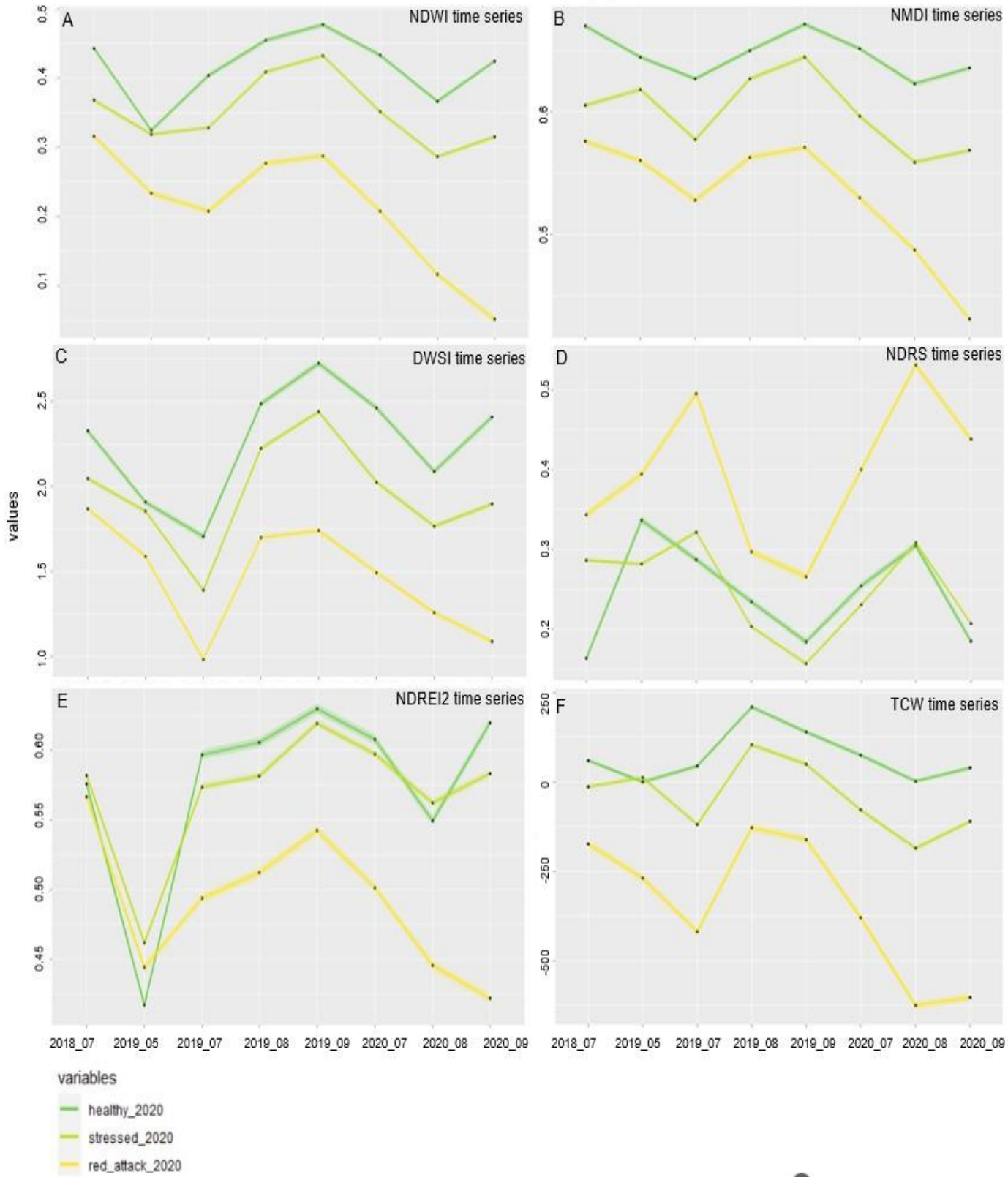

Figure 5. Mean seasonal reflectance trends (line) and standard error (confidence band) of vegetation indices (NDWI, DWSI, NMDI, NDRS, NDREI2 and TCW) from 2018 to 2020 with training data from 2020 for the classes of healthy, stressed and "red_attack" stage canopies.

3.2. Supervised classification

3.2.1. Spectral signatures

Spectral signatures were extracted for the chosen classes of each dataset in order to identify changes in reflectance between bands for each class (Fig. 6). For the visible region of the electromagnetic spectrum, an increase in both green (B03) and red (B04) was found for the "red_attack" stage class, compared to the reflectance values of healthy stands, while the Red-Edge bands (B06 and B07) showed a significant decrease (Fig. 6, A and C). In the SWIR (B11, B12) an increase in reflectance is shown for the "red_attack" class (Fig. 6, A and C). The "stressed" class showed a decrease in reflectance for the green band (B03) towards values of the red band (B04) (Fig. 6, A and C). The Red-Edge region (B05, B06, B07) is characterized by lower reflectance values compared to those of the "healthy" class, while the SWIR bands (B11, B12) were characterized by similar values compared to those of healthy stands (Fig. 6, A and C). The "stressed" class was also the one with the lowest variation for all bands (Fig. 6, B and D).

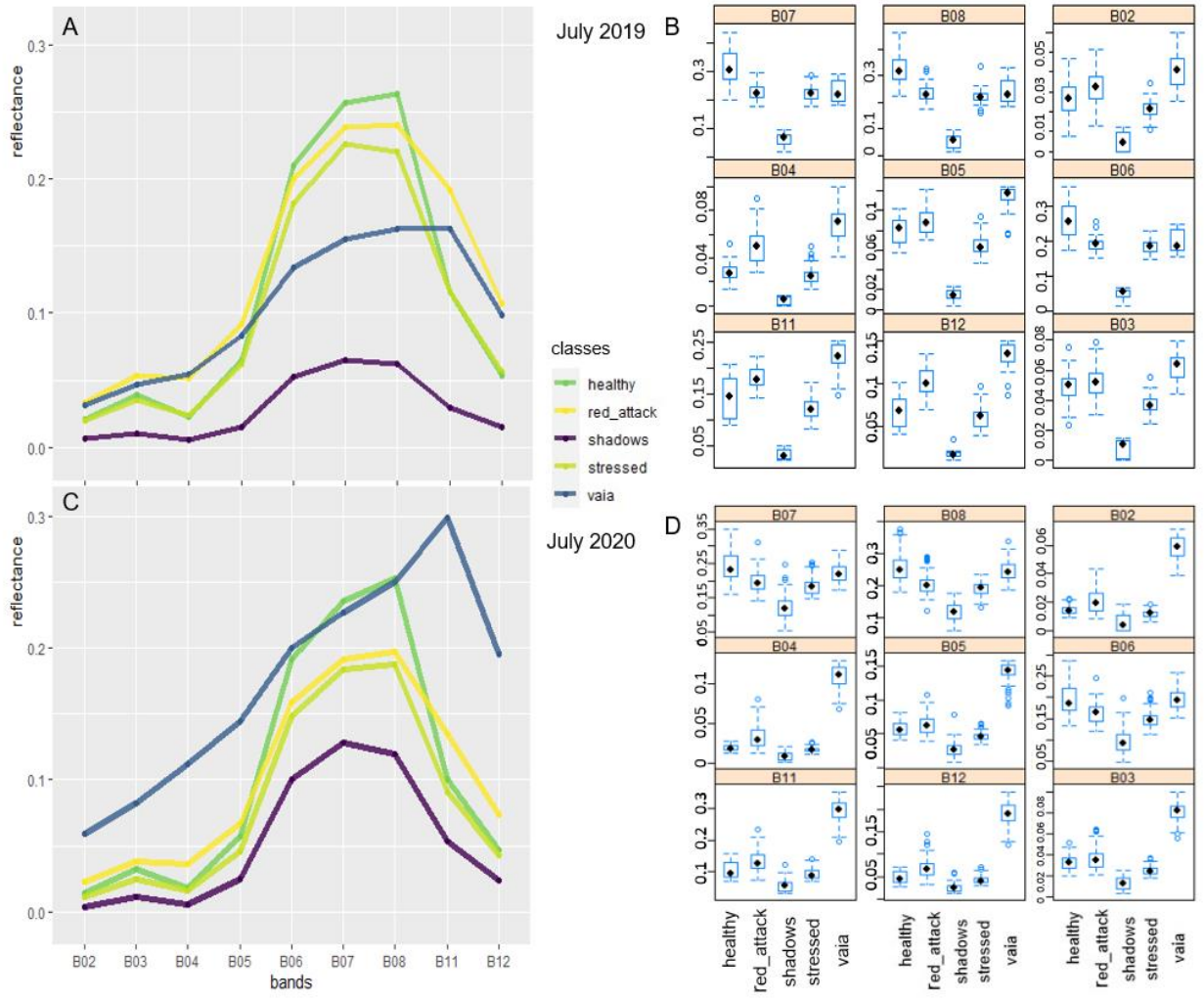

Figure 6. Spectral profiles (A and C) and variation per class for each band (B and D) for July 2019 and July 2020 of forest cover classes (healthy, red_attack, shadows, stressed and Vaia).

3.2.2. Maps of damage

The supervised classification was performed over the entire area of interest at once. For demonstration purposes, we focus on two cropped areas to highlight the classification results (Fig. 7). The maps were compared with validation ground surveys and visual interpretation of orthophotos from 2020 provided by Irdat FVG [43].

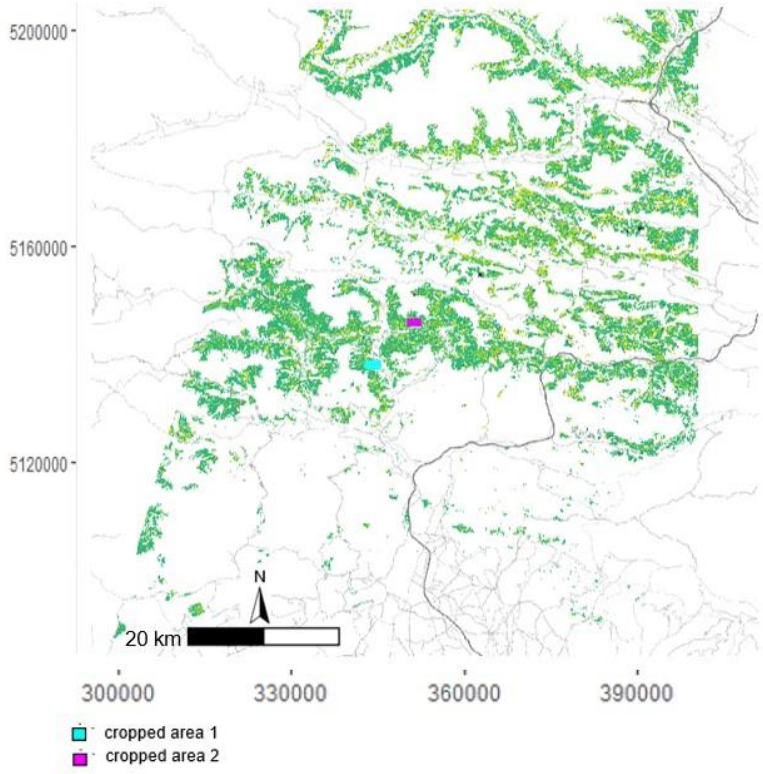

Figure 7. Location of two cropped areas among the study area selected to visualize classification results and changes in forest cover and health. Reference System: WGS84- UTM33N.

Forest stands in the cropped area nr. 1 did already show conditions of stress and "red_attack" stage in June 2017 (Fig. 8, A). The sites detected as stressed in June 2017 (Fig. 8, A), were classified as "red_attack" stage stands in the classification map of July 2018 (Fig. 8, B). The area was already suffering from bark beetle infestations before the Vaia storm occurred, however a significant increase in damage can be seen in the "after Vaia" situation in 2019 and 2020, especially beginning in September 2019 (Fig. 8, E) and July 2020 (Fig. 8, F). Some of the stands which were already stressed in May 2019 (Fig. 8, C), changed into "red_attack" stage in July 2019 (Fig. 8, D) and others in September of 2019 (Fig. 8, E). Not all of the stands detected as stressed turned into "red_attack" stage, but all those which eventually turned out to have been infested by bark beetles had previously been classified as stressed. The bark beetle spread that occurred after the Vaia storm, progressed along forest edges and/or in proximity to wind fell patches (Fig. 8, D, E and F). At the same time, according to classification results (Fig. 8), forest stands wich suffered damage from Vaia were located along forest edges and/or next to forest stands that were already suffering from bark beetle infestations before the storm occurred.

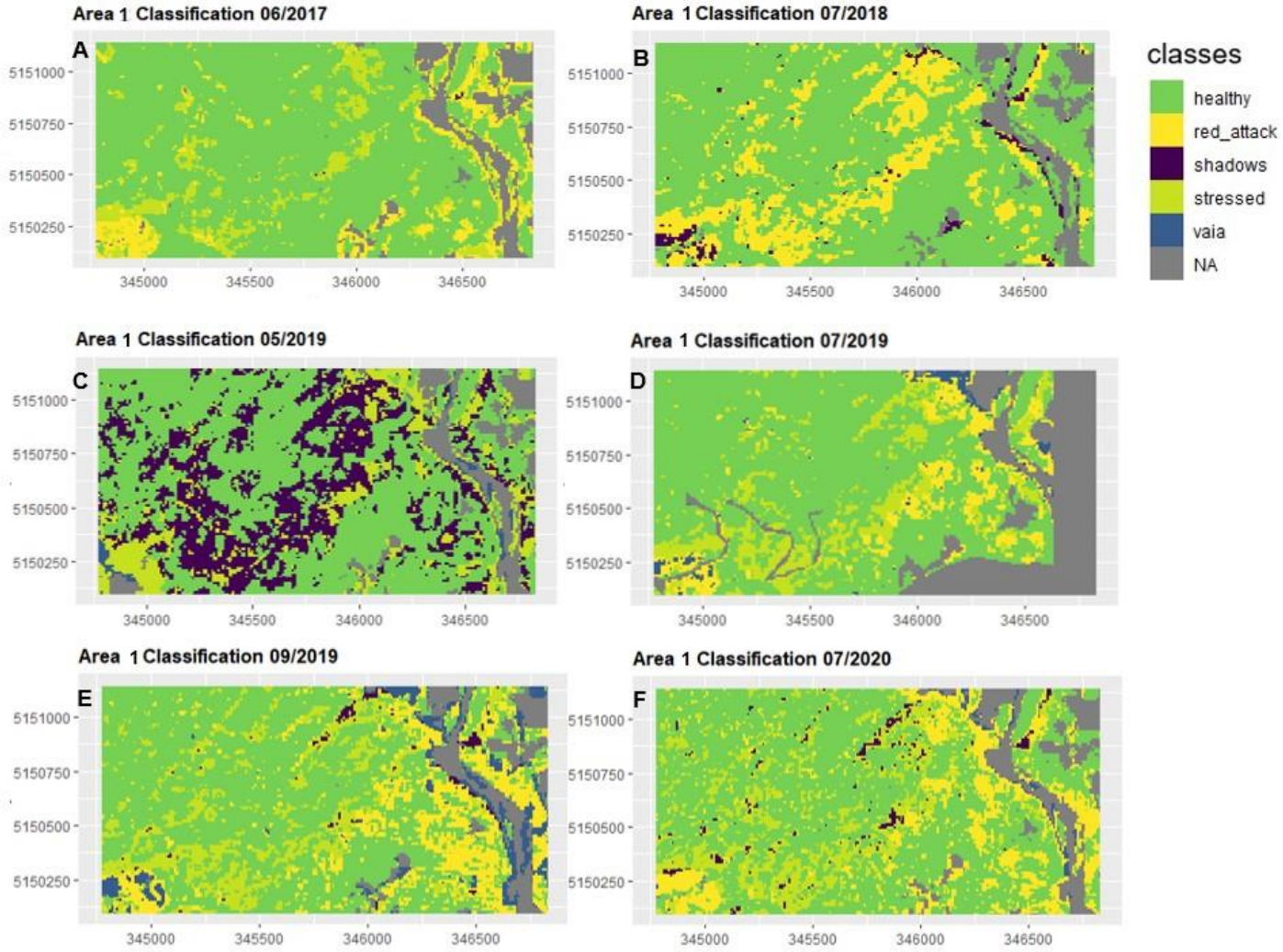

Figure 8. Classification maps of cropped area 1 from 2017 to 2020 (June 2017, July 2018, May 2019, July 2019, September 2019 and July 2020) according to forest cover classes (healthy, red_attack, shadows, stressed, vaia). Reference System: WGS84- UTM33N.

As for the cropped area nr. 1, also the forest stands of the cropped area 2 (Fig. 9) did already show conditions of stress and "red_attack" stage in June 2017 (Fig. 9, A). The sites detected as stressed in June 2017 (Fig. 9, A), were classified as "red_attack" stage stands in the classification map of July 2018 (Fig. 9, B). Some of the canopies detected as stressed in May 2019 (Fig. 9, C), turned into the "red_attack" stage class already in July 2019 (Fig. 9, D), while most of them changed class in September 2019 (Fig. 9, E) or even in the following season (Fig. 9, F). Orthophoto details from 2020 showed how several forest stands located nearby wind fell areas (top-right corner of the orthophoto details), were classified as stressed in 2019 (Fig. 9, C, D and E) and how they turned into "red_attack" stage in July 2020 (Fig. 9, F). According to classification results, bark beetle infestations generally intensified after Vaia storm, especially in 2020, two years after the event (Fig. 9, F) and spread in proximity to wind fell patches (Fig. 9, E).

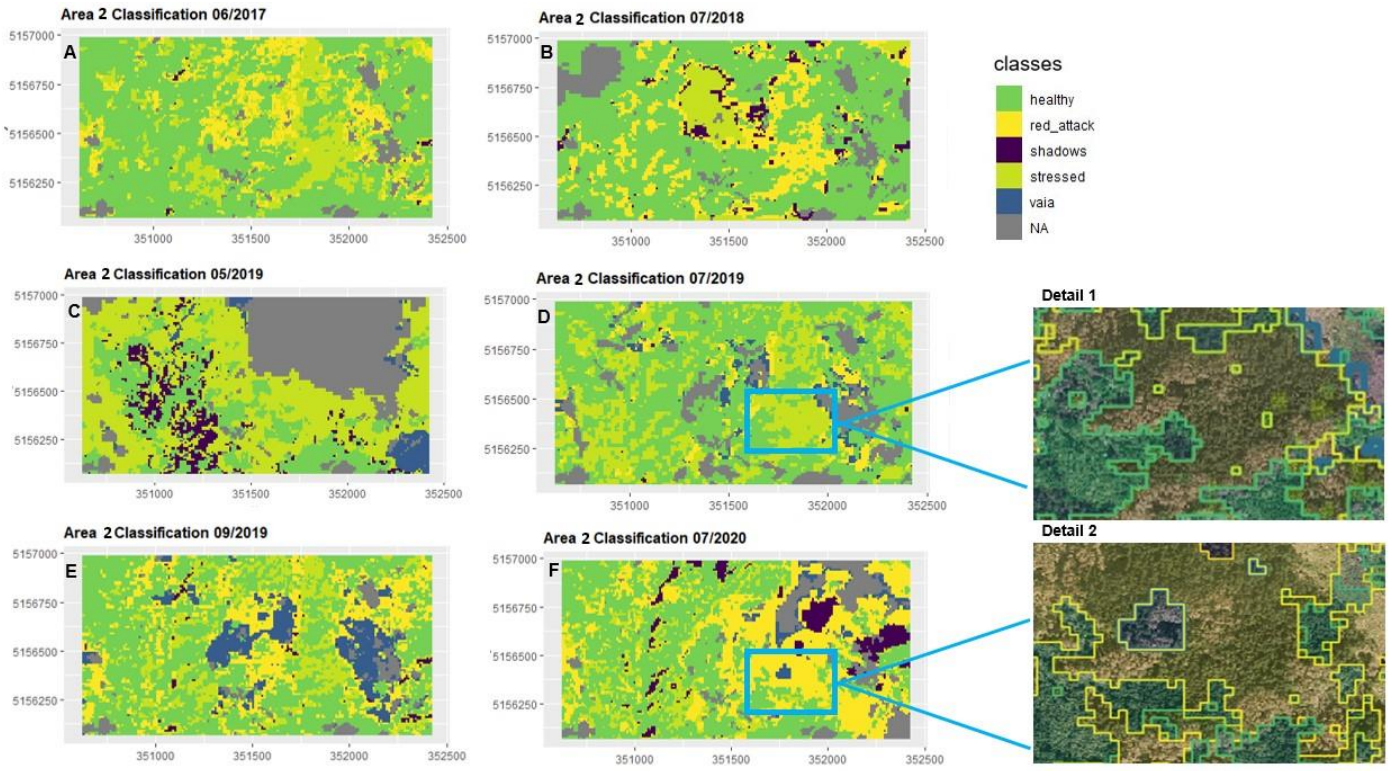

Figure 9. Classification maps of cropped area 2 (June 2017, July 2018, May 2019, July 2019, September 2019 and July 2020) according to forest cover classes (healthy, red_attack, shadows, stressed, vaia) and details showing orthophotos from 2020 with a spatial resolution of 10 cm provided by IRDAT. The orthophotos were overlayed by classification products in form of polygons and transparent rasters. Reference System: WGS84- UTM33N.

Overall accuracies of all supervised classifications reported varied between 0.8 and 1 with Kappa values between 0.7 and 1 (Appendix Fig. A1). Variable importance slightly varied between the different classification algorithms of which ANN and RF resulted to be the most suitable for forest health detection and forest cover change detection. The most important variables for ANN classifications were the Red Edge band (B06) and the Green band (B03) as well as vegetation indices containing the Red Edge bands like NDREI1, NDREI2 and REIP (Fig. 10, B, D, F, H, J and L). The RF algorithm relied mostly on the Red Edge band (B06) and on the NIR band (B08) and on the NDRS index containing the Red (B04) and the SWIR (B12) band, as well as on vegetation indices containing the Red Edge bands (NDREI2, REIP) (Fig. 10, A, C, E, G, I and K).

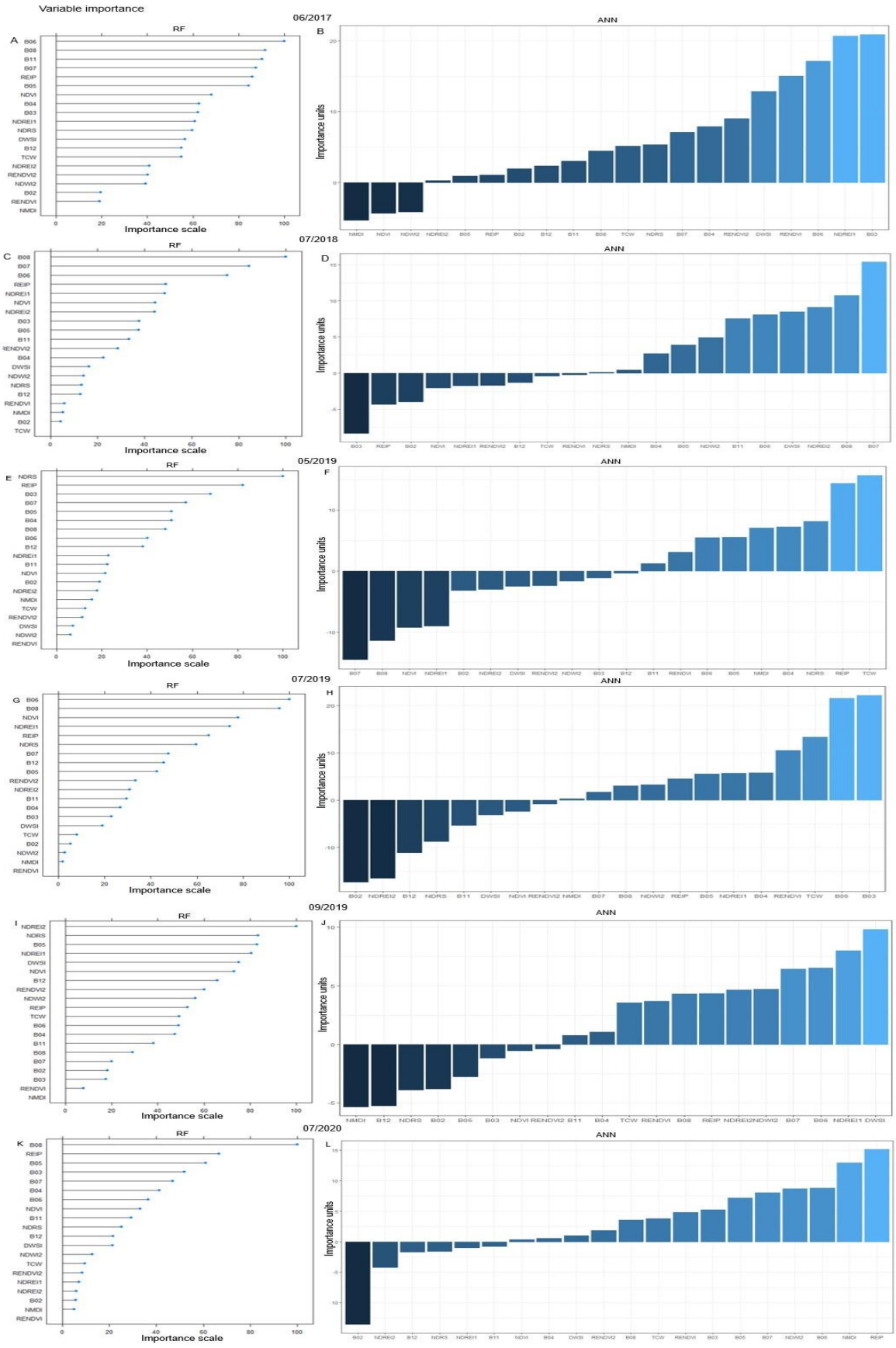
Variable importance
06/2017
07/2018
05/2019
07/2019
09/2019
07/2020
RF
ANN
A
B
C
D
E
F
G
H
I
J
K
L
Importance scale
Importance units

Figure 10. Variable importance for RF and ANN for each classification dataset. Importance values for each explanatory variable for RF are expressed in a scale from 0 to 100 and were calculated with the R "caret" package (version 6.0.91). Variable importance for ANN was calculated with the R "NeuralNetTools" package (version 1.5.3) based on relative importance of input variables in neural networks as the sum of the product of raw input-hidden, hidden-output connection weights, proposed by Olden et al. [55]. The importance values assigned to each variable are in units that are based directly on the summed product of the connection weights. The actual values should only be interpreted based on relative sign and magnitude between explanatory variables. Comparisons between different models should not be made [55].

3.4. Post-Classification change detection

Considering forest cover changes that occurred in cropped areas 1 and 2 affected by both Vaia and bark beetle infestation damage, while the first change, represented in yellow, includes damages by both Vaia and bark beetles, the second change, represented in red, was caused only by bark beetle damage (Fig. 11, A and C). Cropped area 1 witnessed a change in forest cover of approximately 36% in the two years following the Vaia storm (Fig. 11, A), while cropped area 2 suffered a decrease in forest health of 65% from 2018 to 2020 (Fig. 11, C). As shown by classification results and ground monitoring, we could confirm that both areas experienced an increase in bark beetle damage in the two years following the Vaia storm (mostly in 2020) compared to the before Vaia situation in 2018 (Fig. 11, B and D). In both cases several forest stands were already suffering from stress in 2018, a year characterized by particular high drought and low levels of precipitation [34, 38], which lead to a further increase in stressed canopies in 2019 (Fig. 11, B and D).

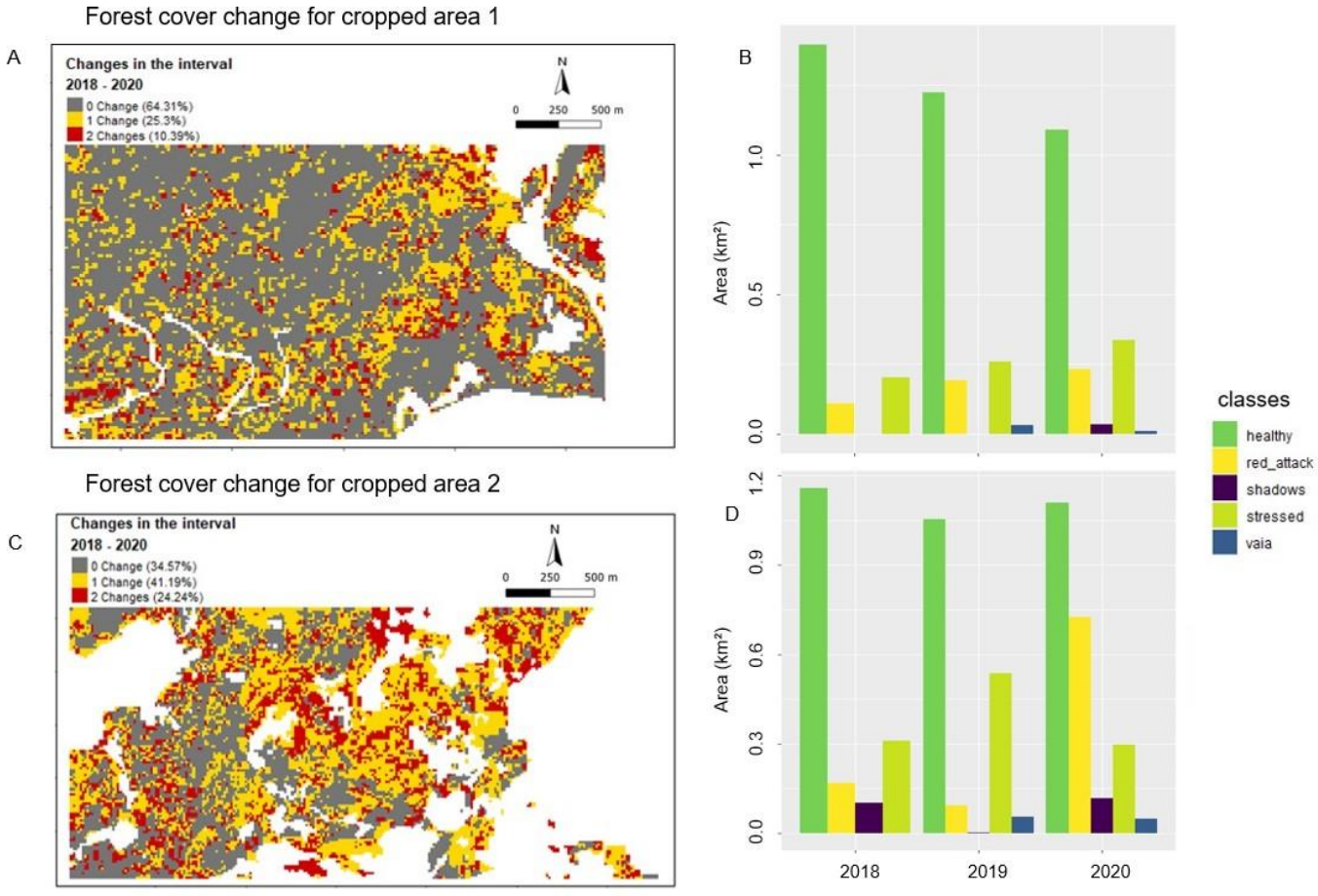

Figure 11. Forest cover change maps in % (A and C) and land cover change per class in km² (B and D) for cropped areas 1 and 2 from 2018 to 2020 according to forest cover classes (healthy, red_attack, shadows, stressed and Vaia).

4. Discussion

According to the study results, Sentinel-2 data resulted suitable for the evaluation of forest health (forest condition before, during, and after the disturbance events) and the process of forest decline is detectable at the spatial resolution of a Sentinel-2 pixel. For this reason, the study areas represent a forest under different circumstances and development (Vaia storm damages, stressed forest stands, infested and dead trees after a bark beetle outbreak and the forest vegetation without any significant influence). We could quantify an increase in forest loss after Vaia storm, which triggered the outbreak of bark beetle populations (Fig. 8, 9 and 11), also induced by increasing temperatures, low spring precipitations and drought, as indicated by climate reference data [28-34]. This scenario confirms that stands already suffering from biotic disturbances (e.g. bark beetles) are weakened and predisposed to suffer further damages in case of abiotic disturbances (e.g. wind storms and drought), while those, again, trigger bark beetle infestations. This is consistent with previous studies [3, 4, 12, 56].

The NIR (B08) and the SWIR (B12) band (Fig. 4) as well as vegetation indices NDWI, DWSI, NMDI, NDRS, NDREI, NDREI2 and especially TCW (Fig. 5) were able to distinguish healthy and stressed or damaged forest stands. The Red Edge band (B06) and the NIR (B08) band exhibited the greatest potential for identifying stress and forest change during the classification processes (Fig. 10). This can be explained by the fact that the Red Edge and NIR parts of the electromagnetic spectrum are sensitive to changes in leaf pigment, as well as canopy structure [15]. Red Edge values, found to be useful to estimate chlorophyll concentrations as well as minimizing the effects of background soil reflectance [23]. Furthermore, Red Edge spectral reflectance indices should be used to increase the accuracy of mapping green-attacked trees since they are less correlated with changes in forest structure, needle age, leaf intercellular structure of air-to-cell wall interfaces, forest floor moisture content, and tree physiology over the growing seasons in healthy forests [23]. Vegetation indices relying on the Red Edge (B06 and B07), SWIR (B12) and the Red (B04) bands performed better in identifying stressed forest during classification (Fig. 10). Pixels covering forest stands under bark beetle "red_attack" stage showed an increase in reflectance values in the Red (B04) and SWIR (B12) band (Fig. 6). The reduction in chlorophyll decreases the spectral absorption in the visible region, resulting in higher reflectance especially in the Red band [57]. Further, bark beetle attacks are known to decrease the canopy water content [20], affecting the SWIR part of the spectrum by causing an increase in reflectance [58]. Previous studies indicate that reflectance changes of infested Norway spruce trees were observable especially in the Red-Edge and SWIR regions both for leaf and canopy levels and that spectral vegetation indices calculated from the Red-Edge and SWIR spectral bands were able to differentiate between healthy and infested trees earlier than the other indices [15, 20, 21].

The classification results showed a high mean overall accuracy (89%) (Appendix Fig. A1) for forest stand stress detection and proved the suitability of Sentinel-2 image processing as differences in reflectance can already be detected in comparison to healthy forest stands while there are no visible changes at ground level. Pixels covering forest stands identified as under bark beetle "red_attack" stage already showed symptoms of stress in the previous season (Fig. 4, 5, 8 and 9). Since spectral differences between healthy and stressed trees could very well exist without an ongoing bark beetle infestation, it is insufficient to conclude that green-attack stage was successfully detected with our Sentinel-2 monitoring framework. The results of previous studies [24, 59] indicate that spectral differences can already exist at the beginning of the vegetation season, before the attacks, or even in previous years. The spectral difference existing before attacks may be related to the weakness and stress, which induce the trees to be selected and later successfully infested by the bark beetles [24]. Indeed, a study has shown that these stress-induced spectral changes could be more efficient indicators of early infestations than the green-attack symptoms [24]. Similar spectral trait variation observed for bark beetle attacks is produced by various other types of disturbances [60], however bark beetle spots develop with a certain speed that is greater than most abiotic stresses [61].

The availability of cloud-free Sentinel-2 images is a very important prerequisite for the successful assessment of bark beetle activity. Unfortunately, mountain areas are frequently cloud cover in spring and therefore only two cloud free images were found for the month of May for the study period (Tab. 1). Actually, this period can be used as an initial reference, especially for forest stands showing stress already before being attacked later on in the season or for forest stands affected by infestation from the

previous season. We assume that forest stands classified as under "red_attack" stage in July combine canopies attacked in the previous season and classified as stressed according to our classification results (Fig. 8 and 9, D and F), as well as newly infested trees by the first bark beetle generation, which according to the PHENIPS model started swarming in May [42]. Stands suffering under bark beetle "red_attack" stage in September (Fig. 8 and 9, E), likely correspond to infestations by the second bark beetle generation, which according to the PHENIPS model started swarming in July [42]. A survey conducted in the Southeastern US suggested high activity of bark beetles during June, with observed signs of infestation and spots during August 2019, two months after activity [58]. The period between mid-June to early-July was found to be appropriate for mapping beetle-induced early stressed trees in Central Europe [21]. For this reason, for early estimation of forest vulnerability, Sentinel-2 image processing in late spring and early summer is also of great use to detect spectral differences related to bark beetle green-attack stage or general conditions of weakness and stress in tree canopies, as they could later be selected and successfully infested by bark beetles or harmed by abiotic disturbances. This would theoretically give forest managers sufficient time to proceed with salvage logging [62]. However, due to the current high outbreak levels, it is not feasible to monitor large areas in a sufficiently timely manner [15] and costs for punctual sanitary cuts are not sustainable for the forest management sector, especially in mountain areas [1].

Including information about forest stand structure (e.g., tree age and density) using auxiliary data such as biomass maps, tree species maps and stand attribute tables [24] and relying only on pure Norway spruce forest stands rather than forest mixtures, would most likely increase the accuracy of overall results and even more the ability for early detection of infestations. Furthermore, according to a previous study [63], the accuracy of infestation detection severely decreases with the decreasing number of infested trees within a mixed pixel. A real qualitative change could already be brought by an improvement in the spectral or spatial resolution, as shown by the discussion of the results or the non-pixel but object-oriented approach, in which not only information from a given pixel is analyzed, but also the context in which it is located [64]. Despite that, the general idea of this research was to perform image processing on an area with a very large extent and by including mixed spruce strands in order to test Sentinel-2 suitability for early stress detection and general forest cover change detection over wide areas affected by abiotic and biotic disturbances. In addition to generating static bark beetle infestation maps, the spatial spread could also be predicted by including data such as wetness and brightness slope, which improved the predictive ability of bark beetle infestation models in a recent study [65]. The proportion of stand borders exposed to the south and west should also be considered as they are more susceptible to bark beetle attacks [8]. Furthermore, attacks frequently occur at sites with higher vegetation surface temperature at the border of forest stands where exposure to the sunlight creates warmer conditions [20]. Accurate and high-resolution data about soil moisture and land surface temperature could significantly improve the predictive ability of bark beetle infestation models [66, 67]. Therefore interpolated SWI and LST data from currently available low resolution open-access imagery and evapotranspiration data [68] and prediction models such as PHENIPS-TDEF [69] could be implemented. Information about solar radiation, rather than commonly used meteorological variables, since increasing canopy surface temperature was found at attacked stands, are also recommended in a future research outlook for early bark beetle infestation detection [20, 70].

5. Conclusions

The results of this research confirmed that windstorms, especially in relation to increasing temperatures and drought conditions caused by climate change, trigger bark beetle infestations. The multi-temporal remote sensing analysis conducted with Sentinel-2 data resulted useful to study trajectories of forest canopies according to their health status. Single bands, vegetation indices and supervised image classifications were able to discriminate between areas affected by stress and bark beetle compared to those of healthy forest stands. Our results suggest that remote monitoring is suitable for providing spatial information about stressed stands already at an early stage while there are no visible changes at canopy level, but changes can be detected in spectral signatures beyond the visible spectrum. Overall, the results obtained by processing a Sentinel-2 multi-temporal series confirmed its suitability for early stress detection of forest stands and the evaluation of forest cover

change over wide areas affected by both abiotic and biotic disturbances. Still, there is need for further research for an early and accurate detection of bark beetle attacked forest stands in order to distinguish it from other stress factors and which is mandatory for operational application of remote monitoring to be implemented in bark beetle control strategies on large scale. The advantage of the methodology described in this research is its global and large-scale applicability to monitor forest health and accessible according to the FAIR principles [71]. This is an initial but necessary step for better understanding bark beetle population dynamics and thus to develop strategies suitable for constraining massive bark beetle outbreaks, considering that abiotic and biotic disturbances are predicted to frequently occur in the future under the impacts of climate change.

Acknowledgments: We kindly thank the Regional Forestry Service and the Regional Agency for Rural Development (ERSA) of the Autonomous Region Friuli Venezia Giulia and the Carinthian Institute for Geographic Information Systems (KAGIS) for providing reference data regarding bark beetle traps and damage as well as wind felled areas.

Conflicts of Interest: The authors declare no conflict of interest. The funders had no role in the design of the study; in the collection, analyses, or interpretation of data; in the writing of the manuscript, or in the decision to publish the results.

Appendix

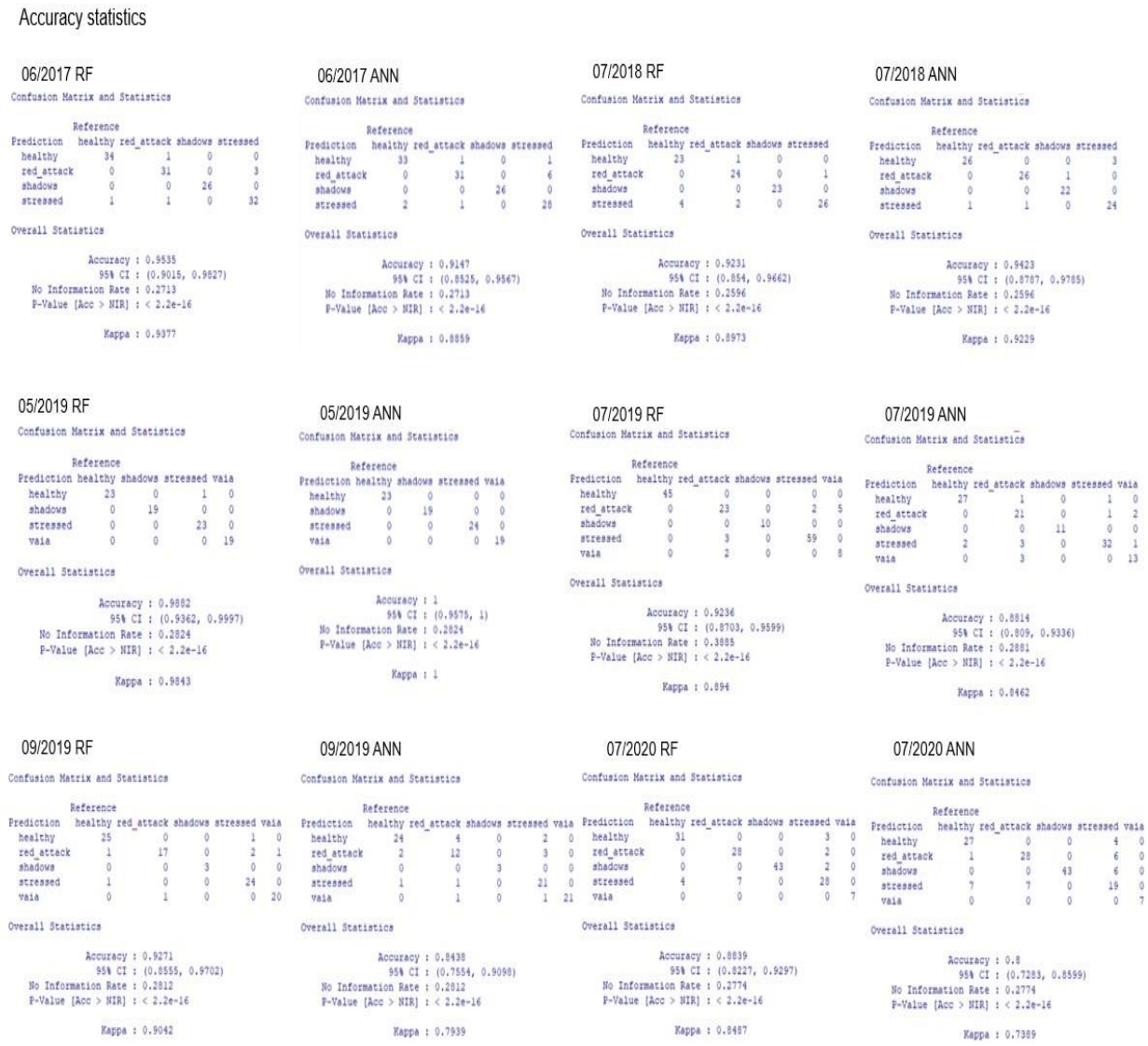

Figure A1. Confusion matrices and overall accuracies for RF and ANN for each classification dataset.

References

1. Gandhi, K.J.; Hofstetter, R.W. *Bark Beetle Management, Ecology and Climate Change*, 1th ed.; Academic Press: London, United Kingdom, 2021
2. Niemann, K.O.; Quinn, G.; Stephen, R.; Visintini, F.; Parton, D. Hyperspectral Remote Sensing of Mountain Pine Beetle with an Emphasis on Previsual Assessment. *Canadian Journal of Remote Sensing* **2015**, *41*, 191-202.
3. Seidl, R.; Thom, D.; Kautz, M.; Martin-Benito, D.; Peltoniemi, M.; Vacchiano, G.; Wild, J.; Ascoli, D.; Petr, M.; Honkaniemi, J.; Lexer, M. J.; Trotsiuk, V.; Mairota, P.; Svoboda, M.; Fabrika, M.; Nagel, T. A.; Reyer, C. P. Forest disturbances under climate change. *Nature Climate Change* **2017**, 7, 6, 395-402
4. Huang, J.; Kautz, M.; Trowbridge, A.M.; Hammerbacher, A.; Raffa, K.F.; Adams, H.D.; Goodsman, D.W.; Xu, C.; Meddens, A.J.; Kandasamy, D.; Gershenzon, J.; Seidl, R.; Hartmann, H. Tree defense and bark beetles in a drying world: carbon partitioning, functioning and modelling. *New Phytologist* **2020**, *225*, 26-36**.**

5. Montzka, C.; Bayat, B.; Tewes, A.; Mengen, D.; Vereecken, H. Sentinel-2 Analysis of Spruce Crown Transparency Levels and Their Environmental Drivers After Summer Drought in the Northern Eifel (Germany). *Front. For. Glob. Change* **2021**, *4*, 1-15.
6. Morris, J.L.; Cottrell, S.; Fettig, C.J.; Hansen, W.D.; Sherriff, R.L.; Carter, V.A.; Clear, J.L.; Clement, J.; DeRose, R.J.; Hicke, J.A.; Higuera, P.E.; Mattor, K.M.; Seddon, A.W.; Seppä, H.T.; Stednick, J.D.; Seybold, S.J. Managing bark beetle impacts on ecosystems and society: priority questions to motivate future research. *J Appl Ecol.* **2017**, *54*, 750-760.
7. Dobor, L.; Hlásny, T.; Zimová, S. Contrasting vulnerability of monospecific and species-diverse forests to wind and bark beetle disturbance: The role of management. *Ecology and Evolution* **2020**, *10(21)*, 12233-12245**.**
8. Wermelinger, B. Ecology and management of the spruce bark beetle *Ips typographus* - a review of recent research. *For. Ecol. Manag*. **2004**, *202*, 67–82.
9. Niemann, K.O.; Visintini, F. Assessment of Potential for Remote Sensing Detection of Bark Beetle-Infested Areas during Green Attack: A Literature Review; Mountain Pine Beetle Initiative Working Paper **2005**-02; Natural Resources Canada; Canadian Forest Service; Pacific Forestry Centre: Victoria, BC, Canada, **2005**
10. White, J.; Wulder, M.; Brooks, D.; Reich, R.; Wheate, R. Detection of Red Attack Stage Mountain Pine Beetle Infestation with High Spatial Resolution Satellite Imagery. Remote Sens. Environ. **2005**, *96*, 340–351
11. Wulder, M.A.; Dymond, C.C.; White, J.C.; Leckie, D.G.; Carroll, A.L. Surveying Mountain Pine Beetle Damage of Forests: A Review of Remote Sensing Opportunities. *For. Ecol. Manag*. **2006**, *221*, 27–41
12. Hlásny, T.; König, L.; Krokene, P.; Lindner, M.; Montagné-Huck, C.; Müller, J.; Qin, H.; Raffa, K.F.; Schelhaas, M.-J.; Svoboda, M.; et al. Bark Beetle Outbreaks in Europe: State of Knowledge and Ways Forward for Management. Curr. For. Rep. **2021**, 7, 138–165
13. Lechner, A.M.; Foody, G.M.; Boyd, D.S. Applications in Remote Sensing to Forest Ecology and Management. *One Earth* **2020**, *2*, 405-412.
14. Fernandez-Carrillo, A.; Patoˇcka, Z.; Dobrovolný, L.; Franco-Nieto, A.; Revilla-Romero, B. Monitoring Bark Beetle Forest Damage in Central Europe. A Remote Sensing Approach Validated with Field Data. *Remote Sens.* **2020**, *12*, 3634
15. Bárta, V.; Lukeš, P.; Homolová, L. Early Detection of Bark Beetle Infestation in Norway Spruce Forests of Central Europe Using Sentinel-2. *Int. J. Appl. Earth Obs*. Geoinf. **2021**, *100*, 102335
16. Senf, C.; Seidl, R.; Hostert, P. Remote Sensing of forest insect disturbances: Current state and future directions. *Int J Appl Earth Obs Geoinf* **2017**, *60*, 49-60
17. Zarco-Tejada, P.J.; Sepulcre-Cantó, G. Remote sensing of vegetation biophysical parameters for detecting stress condition and land cover changes. *Estudios de la Zona No Saturada del Suelo* **2007**, *8,* 37-44.
18. Carter, G. A. Primary and secondary effects of water content on the spectral reflectance of leaves. *American Journal of Botany* **1991**, *78*, 916–924.
19. Einzmann, K.; Atzberger, C.; Pinnel, N.; Glas, C.; Böck, S.; Seitz, R.; Immitzer, M. Early detection of spruce vitality loss with hyperspectral data: Results of an experimental study in Bavaria, Germany. *Remote Sensing of Environment* **2021**, *266*, 112676.
20. Abdullah, H.; Skidmore, A.K.; Darvishzadeh, R.; Heurich, M. Sentinel-2 Accurately Maps Green-Attack Stage of European Spruce Bark Beetle (Ips typographus, L.) Compared with Landsat-8. *Remote Sens. Ecol. Conserv.* **2019**, *5*, 87–106.
21. Abdullah, H. Remote sensing of European spruce (*Ips typographus*, L.) bark beetle green attack. Dissertation, University of Twente, Twente, 2019.
22. Lastovicka, J.; Svec, P.; Paluba, D.; Kobliuk, N.; Svoboda, J.; Hladky, R.; Stych, P. Sentinel-2 Data in an Evaluation of the Impact of the Disturbances on Forest Vegetation. *Remote Sens.* **2020**, *12*
23. Zabihi, K.; Surovy, P.; Trubin, A.; Singh, V.V.; Jakus, R. A review of major factors influencing the accuracy of mapping green-attack stage of bark beetle infestations using satellite imagery: Prospects to avoid data redundancy. *Remote Sensing Applications: Society and Environment* **2021**, *24*
24. Huo, L.; Persson, H.J.; Lindberg, E. Early Detection of Forest Stress from European Spruce Bark Beetle Attack, and a New Vegetation Index: Normalized Distance Red & SWIR (NDRS). *Remote Sens. Environ.* **2021**, *255*, 112240
25. Bernardinelli, I.; Stergulc, F.; Frigimelica, G.; Zandigiacomo, P.; Faccoli, M. Spatial analysis of *Ips Typographus* Infestations in South-Eastern Alps. IUFRO Working Party 7.03.10: **7th Workshop on**

Methodology of Forest Insect and Disease Survey in Central Europe, Gmunden, Austria, 11-14 September 2006.
26. Del Favero, R. *La Vegetazione forestale e la silvicoltura nella Regione Friuli Venezia Giulia*, 1st ed.; Colophon: Friuli Venezia Giulia, Italy, 1998.
27. Seger, M., *Waldschadensforschung im Gailtal, Kärnten. Erfassung des Waldzustandes mittels Farbinfrarot-Fernerkundung und standort- sowie immissionsökologische Ansätze zur Ursachenforschung*, Carinthia II: Klagenfurt, Austria, 1994; pp. 555-625.
28. Regione Autonoma Friuli Venezia Giulia, Arpa, FVG. Available online: https://www.arpa.fvg.it/temi/temi/meteo-e-clima/sezioni-principali/clima-e-cambiamenti-climatici/clima/ (accessed on 07 July 2022)
29. ZAMG, Zentralanstalt für Meteorologie und Geodynamik. Available online: https://www.zamg.ac.at/cms/de/forschung/klima/klimatografien/klimaatlas-kaernten (accessed on 07 July 2022)
30. Unione Meteorologica del Friuli Venezia Giulia. Available online: https://www.umfvg.org/drupal/sites/default/files/Meteorologica-2019-01_02-compresso.pdf (accessed on 07 July 2022)
31. Regione Autonoma Friuli Venezia Giulia, Arpa, FVG. Available online: https://www.arpa.fvg.it/temi/temi/meteo-e-clima/news/e-online-il-report-meteofvg-dedicato-al-2019-un-anno-molto-caldo-con-piogge-abbondanti-in-autunno/ (accessed on 07 July 2022)
32. Regione Autonoma Friuli Venezia Giulia, Arpa, FVG. Available online: https://www.arpa.fvg.it/temi/temi/meteo-e-clima/news/2020-un-anno-caldo-con-piogge-eccezionali-a-dicembre-il-riepilogo-nel-report-annuale-meteofvg/ (accessed on 07 July 2022)
33. Faccoli, M. Effect of weather on Ips typographus (Coleoptera Curculionidae) phenology, voltinims, and associate spruce mortality in the southeastern Alps. *Environ Entomol*. **2009**, *38*, 307-316.
34. Regione Autonoma Friuli Venezia Giulia, Arpa, FVG. Available online: https://www.meteo.fvg.it/pubblicazioni/meteo-fvg//2018/meteo.fvg_2018-5_it.pdf (accessed on 07 July 2022)
35. Chirici, G.; Giannetti, F.; Travaglini, D.; Nocentini, S.; Francini, S.; D'Amico, G.; Calvo, E.; Fasolini, D.; Broll, M.; Maistrelli, F.; Tonner, J.; Pietrogiovanna, M.; Oberlechner, K.; Andriolo, A.; Comino, R.; Faidiga, A.; Pasutto, I.; Carraro, G.; Zen, S.; Contarin, F.; Alfonsi, L.; Wolynski, A.; Zanin, M.; Gagliano, C.; Tonolli, S.; Zoanetti, R.; Tonetti, R.; Cavalli, R.; Lingua, E.; Pirotti, F.; Grigolato, S.; Bellingeri, D.; Zini, E.; Gianelle, D.; Dalponte, M.; Pompei, E.; Stefani, A.; Motta, R.; Morresi, D.; Garbarino, M.; Alberti, G.; Valdevit, F.; Tomelleri, E.; Torresani, M.; Tonon, G.; Marchi, M.; Corona, P.; Marchetti, M. Stima dei danni della tempesta "Vaia" alle foreste in Italia. *Forest@* **2019**, *16*, 3-9
36. Motta, R.; Ascoli, D.; Corona, P.; Marchetti, M.; Vacchiano, G. Selvicoltura e schianti da vento. Il caso della "tempesta Vaia". *Forest@* **2018**, *15*, 94-98
37. European Space Agency. *Sentinel-2 Level-2A Algorithm Theoretical Basis Document*; European Space Agency: Paris, France, 2020.
38. European Space Agency. *Sentinel-2 User Handbook;* European Space Agency: Paris, France, 2015.
39. Regione Autonoma Friuli Venezia Giulia, Ersa, Bausinve 2020. Available online: http://www.ersa.fvg.it/cms/aziende/monitoraggi/bausive/materiale/ (accessed on 07 July 2022)
40. Copernicus Land Monitoring Service. Available online: https://land.copernicus.eu/ (accessed on 07 July 2022)
41. Regione Autonoma Friuli Venezia Giulia, Ersa, Bausinve 2019. Available online: http://www.ersa.fvg.it/cms/aziende/monitoraggi/bausive/materiale/ (accessed on 07 July 2022)
42. Institut für Forstentomologie, Forstpathologie und Forstschutz. Monitoring und Risikoanalyse. Phenips Online Monitoring. Available online: https://ifff-server.boku.ac.at/wordpress/index.php/language/de/startseite/phenips-online/ (accessed on 07 July 2022)
43. Regione Autonoma Friuli Venezia Giulia, Irdat. Available online: http://irdat.regione.fvg.it/WebGIS/ (accessed on 07 July 2022)
44. NASA, Earthdata Search. Available online: https://search.earthdata.nasa.gov/search (accessed on 07 July 2022)
45. Copernicus Open Access Hub. Available online: https://scihub.copernicus.eu/dhus/#/home (accessed on 07 July 2022)
46. Gao, B. C. NDWI, A normalized difference water index for remote sensing of vegetation liquid water from space. *Remote Sensing of Environment* **1996**, *58*, pp. 257–266.

47. Wang, L.; Qu, J. J. NMDI: A normalized multi-band drought index for monitoring soil and vegetation moisture with satellite remote sensing. *Geophysical Research Letters* **2007**, 34
48. Zbigniew, B.; Ziolkowski, D.; Bartold, M.; Orlowska, K.; Ochtyra, A. Monitoring forest biodiversity and the impact of climate on forest environment using high-resolution satellite images. *European Journal of Remote Sensing* **2018**, *51*, 166-181.
49. Chen, G.; Meentemeyer, R. K. Remote Sensing of Forest Damage by Diseases and Insects. In *Remote Sensing for Sustainability*; Weng, Q.; CRC Press: Boca Raton, Florida, USA; 2016, pp. 145-157.
50. Evangelides, C.; Nobajas, A. Red-Edge Normalised Difference Vegetation Index (NDVI705) from Sentinel-2 imagery to assess post-fire regeneration. *Remote Sensing Applications: Society and Environment* **2020**, *17.*
51. Cundill, S. L.; Van der Werff, H.M.; Van der Meijde, M. Adjusting Spectral Indices for Spectral Response Function Differences of Very High Spatial Resolution Sensors Simulated from Field Spectra. *Sensors* **2015**, 15.
52. Index Database. A database for remote sensing indices. Available online: www.indexdatabase.de
53. Eastman, J. R. TerrSet manual. Accessed in TerrSet version 2015, 18(1).
54. Aldwaik, S.Z.; Pontius, R.G. Jr. Intensity analysis to unify measurements of size and stationarity of land changes by interval, category and transition. *Landscape and Urban Planning* **2012**, *106*, 103-114.
55. Olden, J.D.; Joy, M.K.; Death, R.G. An accurate comparison of methods for quantifying variable importance in artificial neural networks using simulated data. *Ecological Modelling* **2004**, *178*, 389- 397.
56. Ochtyra, A. Forest Disturbances in Polish Tatra Mountains for 1985–2016 in Relation to Topography, Stand Features, and Protection Zone. Forests 2020, 11, 579
57. Carter, G.A.; Knapp, A.K. Leaf optical properties in higher plants: linking spectral characteristics to stress and chlorophyll concentration. *Am. J. Bot*. **2001**, *88*, 677-684.
58. Gao, B.C. NDWI – A Normalized difference water index for remote sensing of vegetation liquid water from space. *Remote Sens. Environ.* **1996**, *58*, 257-266.
59. Lausch, A.; Heurich, M.; Dordalla, D.; Dobner, H.J.; Gwillym-Margianto, S.; Salbach, C. Forecasting potential bark beetle outbreaks based on spruce forest vitality using hyperspectral remote-sensing techniques at different scales. *For. Ecol. Manag.* **2013**, *308*, 76-89.
60. Lausch, A.; Erasmi, S.; King, D.J.; Magdon, P.; Heurich, M. Understanding forest health with remote sensing—Part I—A review of spectral traits, processes and remote-sensing characteristics. *Remote Sens. 2016*, 8, 1029.
61. Gomez, D.F; Ritger, H.M.W; Pearce, C.; Eickwort, J.; Hulcr, J. Ability of Remote Sensing Systems to Detect Bark Beetle Spots in the Southeastern US. *Forests* **2020**, *11,* 1167.

62. *Faccoli, M.; Finozzi, V.; Andriolo, A.; Bernardinelli, I.; Salvadori, C.; Deganutti, L.; Battisti, A. Il bostrico tipografo sulle Alpi orientali. Evoluzione, gestione e prospettive future dopo Vaia. SHERWOOD. FORESTE ED ALBERI OGGI* ***2022****, 257, 23-26.*
63. Meddens, A.J.H.; Hicke, J.A.; Vierling, L.A.; Hudak, A.T. Evaluating methods to detect bark beetle-caused tree mortality using single-date and multi-date Landsat imagery. *Remote Sens. Environ.* **2013**, *132*, 49-58.
64. Migas-Mazur, R.; Kycko, M.; Zwijacz-Kozica, T.; Zagajewski, B. Assessment of Sentinel-2 Images, Support Vector Machines and Change Detection Algorithms for Bark Beetle Outbreaks Mapping in the Tatra Mountains. *Remote Sens*. **2021**, *13*, 3314.
65. Hais, M.; Wild, J.; Berec, L.; Bruna, J.; Kennedy, R.; Braaten, J.; Broz, Z. Landsat imagery spectral-trajectories – important variables for spatially predicting the risks of bark beetle disturbance. *Remote Sens*. **2016**, *8*, 687.
66. Hais, M.; Kucera, T. Surface temperature change of spruce forest as a result of bark beetle attack: Remote sensing and GIS approach. *Eur J Forest Res* **2008**, *127*, 327-337.
67. Nardi, D.; Jactel, H.; Pagot, E.; Samalens, J.C.; Marini, L. Drought and stand susceptibility to attacks by the European spruce bark beetle: A remote sensing approach. *Agr Forest Entomol.* **2022**, 1-11.
68. Knowles, J.F. (Institute of Arctic and Alpine Research, University of Colorado Boulder, Colorado, USA; School of Geography and Development, University of Arizona, Arizona, USA); Molotoch, N.P. (Institute of Arctic and Alpine Research, University of Colorado Boulder, Colorado, USA; Deparment of Geography, University of Colorado Boulder, Colorado, USA; Jet Propulsion Laboratory, California Institute of Technology, California, USA). Bark Beetle Impacts on Remotely Sensed Evapotranspiration in the Colorado Rocky Mountains, 2019.

69. Institut für Forstentomologie, Forstpathologie und Forstschutz. Monitoring und Risikoanalyse. Phenips-TDEF – Der Einfluss von Trockenperioden auf das Befallsrisiko durch Buchdrucker. Available online: PHENIPS-TDEF | IFFF-RiskAnalyses (boku.ac.at) (accessed on 07 July 2022)
70. Mezei, P.; Potterf, M.; Skvarenina, J.; Rasmussen, J.G.; Jakus, R. Potential Solar Radiation as a Driver for Bark Beetle Infestation on a Landscape Scale. *Forests* **2019**, *10*, 604.
71. Wilkinson, M.; Dumontier, M.; Aalbersberg, I. The FAIR Guiding Principles for scientific data management and stewardship. *Sci Data* **2016**, *3*, 160018.